Static versus Dynamic Fluctuations in the One-Dimensional Extended Hubbard Model

H.A. Craig[1,2], C.N. Varney[2], W.E. Pickett[2], R.T. Scalettar[2]
[1] *American River College, Sacramento, California 95841, USA and*
[2] *Physics Department, University of California, Davis, California 95616, USA*

The extended Hubbard Hamiltonian is a widely accepted model for uncovering the effects of strong correlations on the phase diagram of low-dimensional systems, and a variety of theoretical techniques have been applied to it. In this paper the World Line Quantum Monte Carlo method is used to study spin, charge, and bond order correlations of the one-dimensional extended Hubbard model in the presence of coupling to the lattice. A static alternating lattice distortion ('ionic Hubbard model') leads to enhanced charge density wave correlations at the expense of antiferromagnetic order. When the lattice degrees of freedom are dynamic (the Hubbard-Holstein model), we show that a similar effect occurs even though the charge asymmetry must arise spontaneously. Although the evolution of the total energy with lattice coupling is smooth, the individual components exhibit sharp cross-overs at the phase boundaries. Finally, we observe a tendency for bond order in the region between the charge and spin density wave phases.

PACS numbers: 071.10.Fd, 71.30.+h, 02.70.Uu

I. INTRODUCTION

The study of strong interaction effects in low-dimensional systems remains one of the most active fields of research in condensed matter physics. The extended Hubbard Hamiltonian (EHH) has been widely explored as a model of correlation effects in tight-binding systems and, more specifically, for the competition between different types of ground state order: charge density wave, antiferromagnetism, and, in the case of attractive interactions, superconductivity. In one dimension, it has also been used to understand the behavior of materials including conducting polymers[1] and organic superconductors[2].

The ground state phase diagram of the one-dimensional EHH was first obtained within a weak coupling renormalization group (RG) calculation[3,4]. For repulsive on-site interactions U which are sufficiently large compared to the intersite repulsion V, specifically, for $U > 2V$, the ground state is a spin density wave (SDW) phase, with power law decay of spin correlations. For $2V > U$, the ground state has charge density wave (CDW) order. These charge correlations exhibit true long range order, that is, they go asymptotically to a non-zero value at large separations, since the associated broken symmetry is discrete. Finally, for attractive intersite interactions, singlet and triplet superconducting phases exist at $T = 0$, again with power law decays of the associated correlation functions.

Subsequent to the RG work, the question of the order of the transitions between these different phases was studied, with a prediction that for repulsive U and V second order SDW-CDW transitions at weak coupling were separated by a tricritical point from first order transitions at strong coupling[5,6,7,8]. Up to several years ago, estimates of the location of the tricritical point varied from $U_t = 1.5t$ to $U_t = 5t$ (with $V_t \approx U_t/2$.) More recently, this picture has been further modified by the suggestion that a narrow region exhibiting 'bond ordered wave' (BOW) correlations separates the SDW and CDW regions at weak coupling[9,10,11]. The precise topology of the BOW region is still under debate.

The competition of CDW and SDW order in the one-dimensional EHH is further modified if the electrons couple to lattice degrees of freedom. In the case where these are static, most investigations have addressed the case when there is only on-site repulsion U, that is, $V = 0$. In this 'ionic Hubbard model' the frozen distortions have an alternating pattern down the chain[12], and an additional issue is the possibility that the band insulator at $U = 0$ and half-filling is first driven metallic before becoming a SDW Mott insulator[13,14]. If the coupling of the electrons to the lattice is in the form of dynamically varying phonon degrees of freedom, one has the 'Hubbard-Holstein' or 'Su-Schrieffer-Heeger' Hamiltonians.

The interplay between band insulating behavior and electron-electron interaction effects such as those studied in this paper has recently been explored in a number of contexts. Dynamical mean field theory studies of binary alloy band insulators described by a bimodal distribution of randomly located one body potentials have observed several novel effects including Mott insulating behavior away from half filling[15,16] and band-insulator to metal transitions driven by increasing on-site repulsion[17]. Analogous studies of interacting bosons in 'superlattice' potentials in which the site energies are modulated have also been used[18,19,20,21,22] to describe experiments on ultra-cold optically trapped (bosonic) atoms[23,24,25,26].

There has been relatively little work, especially using Quantum Monte Carlo (QMC) which addresses how such lattice coupling affects the SDW-CDW phase boundary in the EHH in which both U and V are non-zero. In this paper we undertake such a study, by applying the World-Line QMC (WLQMC) method to the one-dimensional EHH with an additional, one body potential. An explicit description of our Hamiltonian and a brief review of our numerical approach are presented in Sec. II. The lattice potential is first chosen to have a static, alternating pattern (Sec. III). Subsequently, the potential is allowed to

fluctuate dynamically, i.e. we include on-site 'Holstein' phonons (Sec. IV).

II. MODEL AND COMPUTATIONAL METHODS

The extended Hubbard Hamiltonian is

$$\begin{aligned}\widehat{H}_{\rm el} &= \widehat{K} + \widehat{P} \\ \widehat{K} &= -t\sum_{i\sigma}\left(c^\dagger_{i+1,\sigma}c_{i,\sigma} + c^\dagger_{i,\sigma}c_{i+1,\sigma}\right) \\ \widehat{P} &= U\sum_i n_{i,\uparrow}n_{i,\downarrow} + V\sum_i n_i n_{i+1} \ . \end{aligned} \tag{1}$$

Here $c^\dagger_{i,\sigma}, c_{i,\sigma}$, and $n_{i,\sigma}$ are the creation, destruction and number operators respectively for electrons of spin σ at site i of a one-dimensional lattice, and $n_i = n_{i,\uparrow} + n_{i,\downarrow}$. The hopping t determines the kinetic energy (non-interacting band dispersion $\epsilon_k = -2t\cos k$), and is set to $t = 1$. U and V, taken to be positive, are on-site and inter-site repulsions. We will be exclusively interested in the properties of the model at half filling where the number of fermions $N_f = \sum_i n_i = N$, is equal to the number of lattice sites.

We will consider additional couplings to an on-site lattice degree of freedom,

$$\begin{aligned}\widehat{H} &= \widehat{H}_{\rm el} + \widehat{H}_{\rm lattice} \\ \widehat{H}_{\rm ihm} &= \Delta\sum_i (-1)^i n_i \\ \widehat{H}_{\rm Holstein} &= \lambda\sum_i x_i n_i + \sum_i\left(\frac{1}{2}p_i^2 + \frac{1}{2}\omega_0^2 x_i^2\right) \ , \end{aligned} \tag{2}$$

where $\widehat{H}_{\rm lattice}$ can take one of two possible forms: either static (ionic Hubbard model 'ihm') or dynamic ('Holstein'). Analytic and numeric studies on such Hamiltonians are quite numerous[13,14,27,28,29,30,31,32,33,34,35,36,37,38].

It is useful to review the strong coupling ($t = 0$) phase diagram, since when the hopping is non-zero the topology of the phase diagram is rather similar qualitatively and even quantitatively. In the absence of an interaction with the lattice, the SDW phase, which consists of a collection of singly occupied sites, has energy $E^{t=0}_{\rm sdw} = NV$, while the CDW phase has alternating empty and doubly occupied sites, and energy $E^{t=0}_{\rm cdw} = NU/2$. The boundary is given by $V = U/2$. A static lattice distortion Δ breaks the two-fold symmetry of the CDW state and lowers the energy by $N\Delta$ on the preferred sublattice. The resulting boundary is shifted to $V = U/2 - \Delta$.

In the case of coupling to a dynamical phonon, we can construct the $t = 0$ phase diagram by completing the square of the electron-phonon term in the Hamiltonian. The result is an oscillator with the same frequency ω_0 and an equilibrium position shifted by λ/ω_0^2. An attractive on-site interaction $-(\lambda^2/2\omega_0^2)n_{i,\uparrow}n_{i,\downarrow}$, also is generated. Other terms can be absorbed into a shifted chemical potential and energy. As with the static term, the weakening of the on-site U shifts the strong coupling phase diagram in favor of CDW order. If $-(\lambda^2/2\omega_0^2)$ is sufficiently large, pairing correlations can come to dominate, especially in the doped case. We will not work in that parameter regime here.

In order to understand how the quantum fluctuations, which develop as t increases, modify these simple considerations, we employ the World Line Quantum Monte Carlo (WLQMC) method[39]. Consider first the approach for $\widehat{H} = \widehat{H}_{\rm el} + \widehat{H}_{\rm ihm}$. We begin by discretizing the inverse temperature β into intervals $\epsilon = \beta/M$ in the partition function, and approximating the incremental (imaginary) time evolution operator by the product of the exponentials of the kinetic energy and potential energy terms separately.

$$Z = {\rm Tr}\left[e^{-\beta\widehat{H}}\right] \approx {\rm Tr}\left[e^{-\epsilon\widehat{K}}e^{-\epsilon(\widehat{P}+\widehat{H}_{\rm ihm})}\right]^M \ .$$

This 'Suzuki-Trotter' approximation[40,41] introduces errors in measurements[42,43] which are of order the commutator $[\widehat{K},\widehat{P}]$, that is $t\,U\,\epsilon^2$, $t\,\Delta\,\epsilon^2$, and $t\,V\,\epsilon^2$. Except where otherwise noted, we will choose $\epsilon = 0.25$ which is sufficiently small that the systematic Trotter errors in the location of the phase boundary are comparable to those arising from statistical fluctuations in the Monte Carlo sampling and uncertainties associated with finite size scaling.

The construction of a path integral for Z is completed by introducing complete sets of fermion occupation number states $I = \sum |n_{i,\sigma}\rangle_\tau \langle n_{i,\sigma}|_\tau$ both for the trace, and at all imaginary times, i.e. between each product, $e^{-\epsilon\widehat{K}}e^{-\epsilon\left(\widehat{P}+\widehat{H}_{\rm ihm}\right)}$. The exponentials of the terms in $\widehat{P} + \widehat{H}_{\rm ihm}$ immediately act on the eigenstates, replacing all operators by numbers. Thus the weight of a particular occupation number configuration gets a contribution $W_{\rm P}\,W_{\rm ihm}$,

$$\begin{aligned} W_{\rm P}(\{n_{i,\tau,\sigma}\}) &= \exp\Bigg[\epsilon\sum_{i,\tau}\Big(U n_{i,\tau,\uparrow}n_{i,\tau,\downarrow} \\ &\qquad + V(n_{i,\tau,\uparrow}+n_{i,\tau,\downarrow})(n_{i+1,\tau,\uparrow}+n_{i+1,\tau,\downarrow})\Big)\Bigg] \\ W_{\rm ihm}(\{n_{i,\tau,\sigma}\}) &= \exp\left[\epsilon\sum_{i,\tau}\Delta(-1)^i(n_{i,\tau,\uparrow}+n_{i,\tau,\downarrow})\right] \end{aligned}$$

where $\{n_{i,\tau,\sigma}\}$ denotes the space and imaginary time dependent occupation numbers in the collection of intermediate states.

To accomplish the same replacement of operators by numbers for the kinetic energy exponentials, $\widehat{K}$ is further

subdivided (the 'checkerboard decomposition')[39,44] into

$$\begin{aligned}\widehat{K} &= \widehat{K}_{\rm odd} + \widehat{K}_{\rm even} \\ \widehat{K}_{\rm odd} &= -t \sum_{i\ {\rm odd},\sigma} \left(c^\dagger_{i+1,\sigma} c_{i,\sigma} + c^\dagger_{i,\sigma} c_{i+1,\sigma} \right) \\ \widehat{K}_{\rm even} &= -t \sum_{i\ {\rm even},\sigma} \left(c^\dagger_{i+1,\sigma} c_{i,\sigma} + c^\dagger_{i,\sigma} c_{i+1,\sigma} \right) \ .\end{aligned}$$

The expectation value of $\widehat{K}_{\rm odd}$ and $\widehat{K}_{\rm even}$ between the occupation number states $|n_{i,\sigma}\rangle_\tau$ and $\langle n_{i,\sigma}|_{\tau+1}$ then reduces to a product of independent two site problems which can be solved analytically. Since particle number is conserved in each hopping process, the number of electrons on each pair of sites in the two states to the left and to the right of the exponential is identical. Thus the 'world-lines' generated by connecting all occupied sites ($n_{i,\tau,\sigma} = 1$) are continuous. The four non-zero matrix elements are

$$\begin{aligned}\langle\, 00 \,|\, e^{\epsilon t (c^\dagger_1 c_2 + c^\dagger_2 c_1)} \,|\, 00 \,\rangle &= 1 \\ \langle\, 11 \,|\, e^{\epsilon t (c^\dagger_1 c_2 + c^\dagger_2 c_1)} \,|\, 11 \,\rangle &= 1 \\ \langle\, 10 \,|\, e^{\epsilon t (c^\dagger_1 c_2 + c^\dagger_2 c_1)} \,|\, 10 \,\rangle &= \cosh(t\epsilon) \\ \langle\, 10 \,|\, e^{\epsilon t (c^\dagger_1 c_2 + c^\dagger_2 c_1)} \,|\, 01 \,\rangle &= \sinh(t\epsilon) \ .\end{aligned}$$

The product of all these factors over the space-time lattice constitutes a second contribution $W_{\rm K}$ to the weight associated with the configuration. Thus, the total weight is $W_{\rm tot} = W_{\rm P} W_{\rm ihm} W_{\rm K}$.

In the case $\widehat{H} = \widehat{H}_{\rm el} + \widehat{H}_{\rm Holstein}$, the trace and intermediate states include not only fermion occupation labels, but also a complete set of phonon position eigenstates. As with $\widehat{H}_{\rm el}$, the exponential of the phonon kinetic and potential energies is discretized and split apart. The result is that in addition to the electronic contributions $W_P\, W_K$, there is a final phonon piece,

$$W_{\rm Ph}(\{x_{i,\tau}\}) = \exp\left[\frac{1}{2}\epsilon \sum_{i,\tau} \omega_0^2 x_{i,\tau}^2 + \left(\frac{x_{i,\tau+1} - x_{i,\tau}}{\epsilon} \right)^2 \right] \ .$$

Let us then summarize the basic features of the simulation. The degrees of freedom being summed over are two space-time arrays of occupation numbers $n_{i,\tau,\uparrow}$ and $n_{i,\tau,\downarrow}$, and, in the Holstein case, a space-time array of phonon coordinates $x_{i,\tau}$, with $i = 1, 2, ...N$ and $\tau = 1, 2, ...2M$. (The factor of two comes from the checkerboard decomposition.) The total weight of the configuration is $W_{\rm tot} = W_{\rm P} W_{\rm K} W_{\rm Ph}$. The elemental Monte Carlo moves consist of local distortions of the continuous world-lines, together with updates of the phonon degrees of freedom. Moves are accepted/rejected according to the Metropolis algorithm: a random number $0 < r < 1$ is generated and the move is accepted if $r < W'_{\rm tot}/W_{\rm tot}$.

The WLQMC algorithm can suffer from long autocorrelation times. Other approaches such as the stochastic series expansion method[45,46,47] and loop algorithms[48] can be used to speed up the evolution in phase space. Here we confine ourselves only to introducing global moves[49] in the phonon degrees of freedom to address even more serious large autocorrelation times there.

We conclude with a discussion of the observables we will measure. The various components of the energy exhibit sharp features as the phase boundaries are crossed. Real space spin, charge (relative to the mean), and bond operators are defined by

$$\begin{aligned} m(l,\tau) &= n_{l,\tau,\uparrow} - n_{l,\tau,\downarrow} \\ n(l,\tau) &= n_{l,\tau,\uparrow} + n_{l,\tau,\downarrow} - 1 \\ k(l,\tau) &= \sum_\sigma c^\dagger_{l+1,\sigma}(\tau) c_{l,\sigma}(\tau) + c^\dagger_{l,\sigma}(\tau) c_{l+1,\sigma}(\tau) \ .\end{aligned}$$

The associated correlation functions are

$$\begin{aligned} c_{\rm spin}(l,\tau) &= \langle m(l,\tau) m(0,0) \rangle \\ c_{\rm charge}(l,\tau) &= \langle n(l,\tau) n(0,0) \rangle \\ c_{\rm bond}(l,\tau) &= \langle k(l,\tau) k(0,0) \rangle \ ,\end{aligned}$$

where $(0,0)$ is some reference site in our system. The local moment is defined as $\langle m_z^2 \rangle = c_{\rm spin}(0,0)$.

We will also look at the Fourier transforms of these quantities. The equal time spin structure factor is

$$S_{\rm spin}(q) = \frac{1}{N} \sum_l e^{iql} c_{\rm spin}(l,0) \ ,$$

with analogous definitions for $S_{\rm charge}$ and $S_{\rm bond}$. The corresponding zero-frequency susceptibility is

$$\chi_{\rm spin}(q) = \frac{1}{N} \sum_\tau \sum_l e^{iql} c_{\rm spin}(l,\tau) \ ,$$

again with analogous definitions for $\chi_{\rm charge}$ and $\chi_{\rm bond}$.

At half-filling the largest responses in the Hubbard model are at wavevector $q = \pi$. In a disordered phase, $c(l,0)$ decays exponentially to zero with the site separation l, and the structure factor is independent of lattice size N. If true long range order develops, then the structure factor grows linearly with lattice size, with the factor $e^{i\pi l}$ providing the necessary phases so that the oscillating $c(l)$ add constructively. The susceptibility similarly examines the asymptotics in imaginary time, diverging with β when $c(l,\tau)$ remains nonzero for large τ.

III. RESULTS - EXTENDED IONIC HUBBARD HAMILTONIAN

In the extended Hubbard Hamiltonian with $U = 6t$ and $V = 1.5t$, we are well within the SDW phase since $U > 2V$. In Fig. 1 we see that as Δ is increased, the SDW susceptibility decreases and the CDW susceptibility grows. Indeed, $\chi_{\rm cdw}$ rises dramatically in the vicinity of $\Delta = U/2 - V$, as suggested by the strong coupling analysis. The transition becomes increasingly sharp as

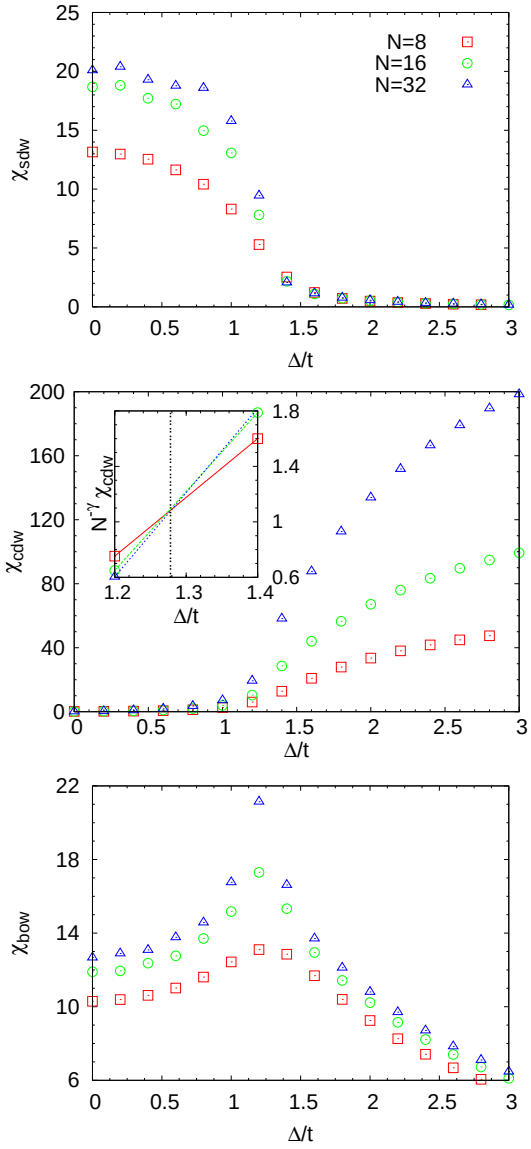

FIG. 1: Spin-density wave (top), charge-density wave (middle), and bond-ordered wave (bottom) susceptibilities versus staggered site energy Δ for $U = 6t$, $V = 1.5t$, $\beta t = 8$, and $N = 8, 16, 32$. The SDW-CDW transition occurs at close to the $t = 0$ value, $\Delta = \frac{1}{2}U - V$. BOW correlations are enhanced in the intermediate region. In the inset to the central panel, the scaled $\chi_{\rm cdw}$ is shown for $\gamma = 1$. The scaled susceptibilities cross at $\Delta_c/t = 1.278$, indicated by the vertical dotted line.

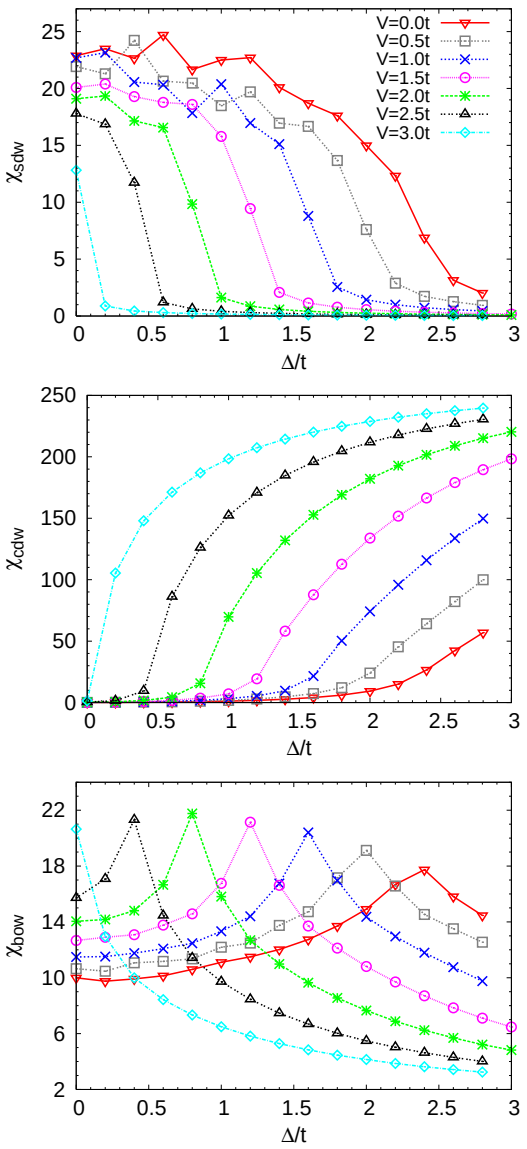

FIG. 2: Spin-density wave (top), charge-density wave (middle), and bond-ordered wave (bottom) susceptibilities versus staggered site energy Δ for $U = 6t$, $V = 0.0t, (0.5t), 3.0t$, and $N = 32$.

the lattice size is increased. Because the CDW correlations break a discrete symmetry, true long range order is possible at $T = 0$. With our normalization conventions we expect the CDW structure factor and susceptibility to grow linearly with lattice size after the onset of long range order. This is borne out in the central panel of Fig. 1. The inset to the central panel shows a scaled version of the raw data for $\chi_{\rm cdw}$. A crossing of the curves for different lattice sizes N allows us to determine the location of the critical point.

The SDW correlations that are dominant at small Δ break a continuous symmetry, and hence in one dimension decay with a power law at $T = 0$, that is $c_{\rm spin}(l, 0) \propto 1/l$. This behavior accounts for the relatively less rapid growth of the SDW susceptibility with lattice size.

It is important to make another distinction between the CDW and SDW phases, the phases that arise as broken symmetries from the interaction terms V and U, and the staggered density which is caused by the one-body term Δ. This staggered potential Δ breaks translational invariance so that there is a small degree of CDW order even in the SDW phase. By contrast, in a competition solely between U and V at $\Delta = 0$, no CDW order would

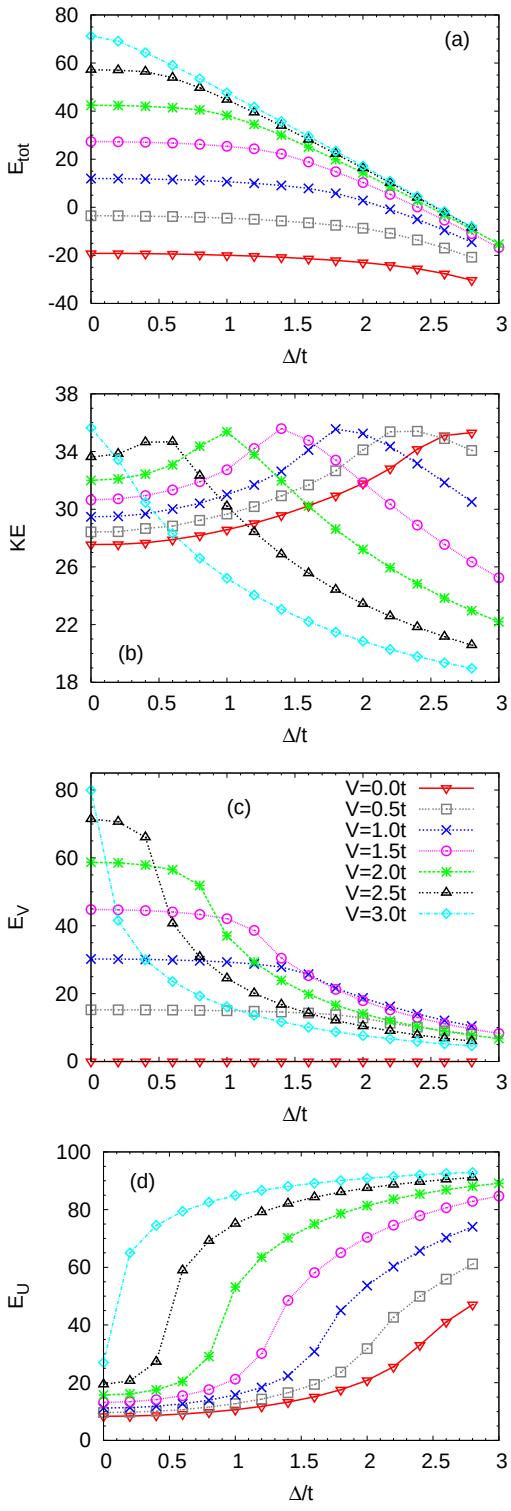

FIG. 3: Total (a), kinetic (b), intersite Coulomb (c) and on-site Coulomb (d) energies at fixed $U = 6t$ and different V. The inverse temperature is fixed at $\beta t = 8$ and the lattice size at $N = 32$. The kinetic energy is largest in the region where there is a balance between the CDW and SDW insulating tendencies, in good correspondence with the behavior of $\chi_{\rm bow}$. The intersite interaction energy falls abruptly on entry to the CDW state, and the on-site energies rise steeply as the pairs form.

exist in the SDW phase.

The bottom panel of Fig. 1 shows the BOW correlations. In a BOW phase the kinetic energy on the links oscillates between two values as one traverses the chain (see Fig. 4). SDW correlations are immediately plausible after observing that U leads to singly occupied sites (moment formation) and that neighboring spins which are antiparallel have a second order lowering of their energy ($\Delta E^{(2)} \propto -t^2/U$) relative to neighboring spins which are parallel. Analogous reasoning applies to CDW correlations. A picture of the less familiar BOW order is the following: consider a CDW pattern of doubly occupied and empty sites. A fermion hopping from doubly occupied site i onto neighboring empty site $i+1$ will prevent, through the interaction U, the hopping of a second electron from doubly occupied site $i+2$ onto $i+1$. Instead, an electron on site $i+2$ would prefer to hop to $i+3$. Thus the bonds $(i, i+1)$ and $(i+2, i+3)$ have high kinetic energy, while the intermediate bond $(i+1, i+2)$ has low kinetic energy. This way of understanding the origin of BO invokes both CDW and SDW correlations, making it plausible that the BOW might form on the boundary between the two.

Since the BOW phase also breaks a discrete translational symmetry, the associated ground state order should be long ranged. As mentioned in the introduction, in the extended Hubbard model ($\Delta = 0$) the original picture of the phase diagram was one with only SDW and CDW regions, with a weak coupling second order transition changing at a tricritical point to a strong coupling first order transition[5,6,7,8]. Recent QMC simulations with the Stochastic Series Expansion (SSE) have suggested instead that at weak coupling as V is increased at fixed U there are two separate transitions: a SDW-BOW transition of the Kosterlitz-Thouless type, followed by a second order BOW-CDW transition. These transitions merge at a multi-critical point into a single, direct, first order SDW-CDW transition line at strong coupling[50]. The multi-critical point was found to be at $(U_m, V_m) = (4.7 \pm 0.1, 2.51 \pm 0.04)$.

Aspects of this conclusion have been challenged by density matrix renormalization group calculations[50,51,52]. In particular, the suggestion is that the BOW phase exists only precisely on the SDW-CDW transition line, as opposed to being present in an extended region. Moreover, rather than starting at $U = V = 0$ and reaching out to the multi-critical point, the BOW line was concluded to begin at finite, nonzero coupling and also extend somewhat beyond the numerical value for the multi-critical point obtained using the SSE.

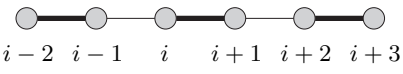

FIG. 4: Illustration of a BOW phase. The thick lines indicate a high kinetic energy whilst the thin lines indicate a small kinetic energy.

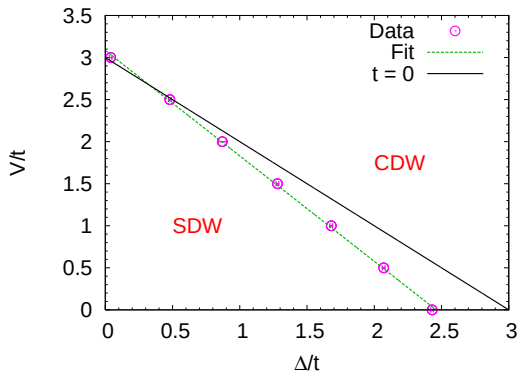

FIG. 5: Phase diagram in the intersite V and staggered site energy Δ plane, with $U = 6t$ and $\beta t = 8$. Line with symbols is the result of the WLQMC simulations in this paper. We also show the exact result (line without symbols) for $t = 0$. As expected, the strong coupling limit works well at large V, but there are significant deviations as V becomes smaller.

We do not propose here to attempt to resolve this difficult issue, since our main focus is on the shift in the SDW-CDW phase boundary. Indeed, the value of U in Fig. 1 is large enough that we would likely be above the BOW region of the phase diagram. Nevertheless, the bottom panel of Fig. 1 does indicate a pronounced maximum in $\chi_{\rm bow}$ near the SDW-CDW transition, hinting that such order may be present at weaker coupling. If long range BO were to exist, we would expect to see $\chi_{\rm bow}$ grow linearly with N, as does $\chi_{\rm cdw}$. This is clearly not the case for the parameters/lattice sizes of Fig. 1.

In Fig. 2 we fix $U = 6t$ and the lattice size at $N = 32$, and sweep Δ for different choices of V. As expected, the size of Δ required to destroy the SDW phase decreases as the intersite interaction V, which cooperates with Δ, rises. As with the data of Fig. 1, the fall of $\chi_{\rm sdw}$ coincides closely with the rise of $\chi_{\rm cdw}$. In each case the transition is marked also by a maximum in $\chi_{\rm bow}$. The sharpness of the peak in $\chi_{\rm bow}$ diminishes as V grows, which is consistent with the SSE[50] and DMRG[51] calculations on the extended Hubbard model which (although they disagree in certain respects) both conclude that BO is not present at strong coupling. We note that a Mott Insulator-BO transition has also been suggested by Zhang *et al.* in the $V = 0$ limit with $\Delta = 2.0$ and $U_c = 5.95 \pm 0.01$[36].

The behavior of the total energy, Fig. 3(a), is featureless through the sweep upwards in Δ. However, abrupt evolution of the individual components of the energy, Fig. 3(b,c,d), accompanies the transitions in the susceptibilities. The energy associated with V decreases sharply upon exiting the SDW phase where adjacent sites are occupied, whilst the energy associated with U jumps upward with the development of double occupancy. The kinetic energy is relatively benign, but, like $\chi_{\rm bow}$, reaches maxima along the SDW-CDW transition line. Evidently, the near balance between the insulating tendencies of U and V allows greater fluctuation in the electron positions.

The values of Δ at which the different susceptibilities change abruptly, and at which features in the energy are also evident, enable us to draw the phase diagram in the $V - \Delta$ plane for fixed $U = 6t$ shown in Fig. 5. At $\Delta = 0$ our QMC results match quite nicely the DMRG results of Jeckelmann[51] who finds $V_c = 3.155 \pm 0.005$ for $U = 6t$. This $\Delta = 0$ transition point is not too far shifted from the strong coupling value $V_c = U/2 = 3t$ when $U = 6t$.

As the staggered potential Δ becomes greater, our QMC phase boundary bends more away from the $t = 0$ line $V_c = U/2 - \Delta$. The SDW phase appears to terminate at $\Delta = 2.46 \pm 0.05$ in the absence of intersite repulsion V. While labeled as CDW, the large Δ phase in the $V = 0$ limit is perhaps more properly termed a band insulator, where the alternating charge density is a consequence of the staggered one-body potential as opposed to many-body effects.

IV. RESULTS - EXTENDED HUBBARD HOLSTEIN HAMILTONIAN

Having completed our discussion of the case of the interplay of a static alternating external potential with the correlation terms U, V in the extended Hubbard Hamiltonian, we now give analogous results for the case when we couple to dynamical (Holstein) lattice distortions. Fig. 6 is a companion to Fig. 1, showing the evolution of the spin-,charge-, and bond-susceptibilities with electron-phonon coupling λ (rather than staggered potential Δ) for different system sizes N. As discussed earlier, λ has a similar qualitative effect to Δ, since it weakens the on-site repulsion U and hence drives CDW formation. There are significant quantitative differences between the two situations. The SDW-CDW transition as a function of electron-phonon coupling λ appears to be much more abrupt. Recall that Δ breaks the lattice symmetry explicitly, selecting out a single preferred sublattice. It induces CDW order even within the SDW phase and as a consequence the change through the transition is less dramatic. The Holstein interaction, in contrast, spontaneously breaks the translational symmetry when it drives CDW order. We note further that BOW order is less sharply peaked at the SDW-CDW boundary.

Fig. 7 is a companion to Fig. 2, similarly showing the susceptibilities as a function of electron-phonon coupling constant λ for a collection of values of V at a single lattice size $N = 32$ and $\omega_0 = 2t$. As V increases, a smaller λ is sufficient to drive CDW formation. There appears to be some variation of the sharpness of the evolution of the susceptibilities near λ_c as V is varied, with the most abrupt behavior occurring for intermediate V. In the extended Hubbard model ($\lambda = 0$) the transitions become monotonically more steep with increasing V. Indeed, as commented earlier they change from continuous to discontinuous beyond the tri-(multi-)critical point. The fluctuations of $\chi_{\rm cdw}$ at large λ in Fig. 7 (middle panel) often occur in QMC studies of electron-phonon Hamil-

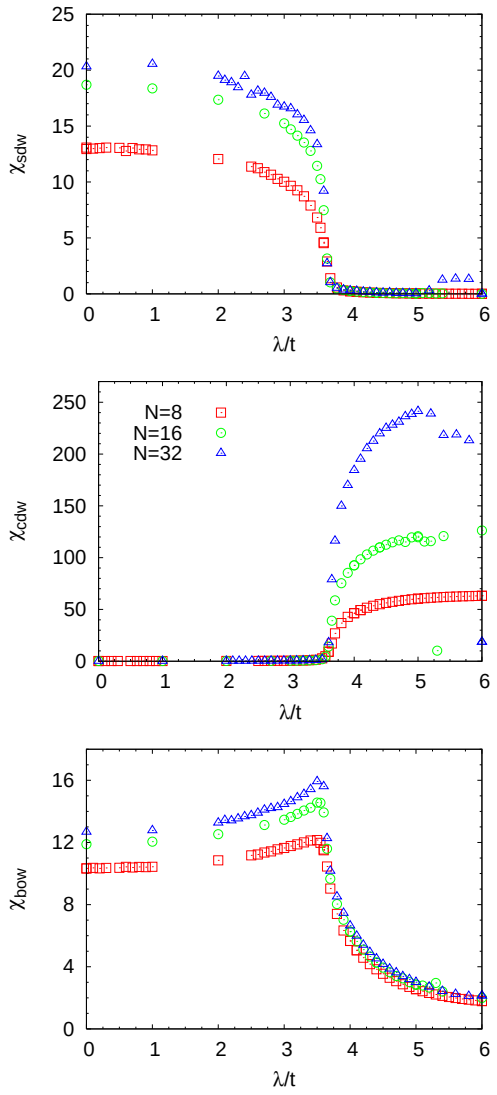

FIG. 6: Spin-density wave (top), charge-density wave (middle), and bond-ordered wave (bottom) susceptibilities versus electron-phonon coupling λ for $U = 6t$, $V = 1.5t$, $\omega_0 = 2t$, $\beta t = 8$, and $N = 8, 16, 32$.

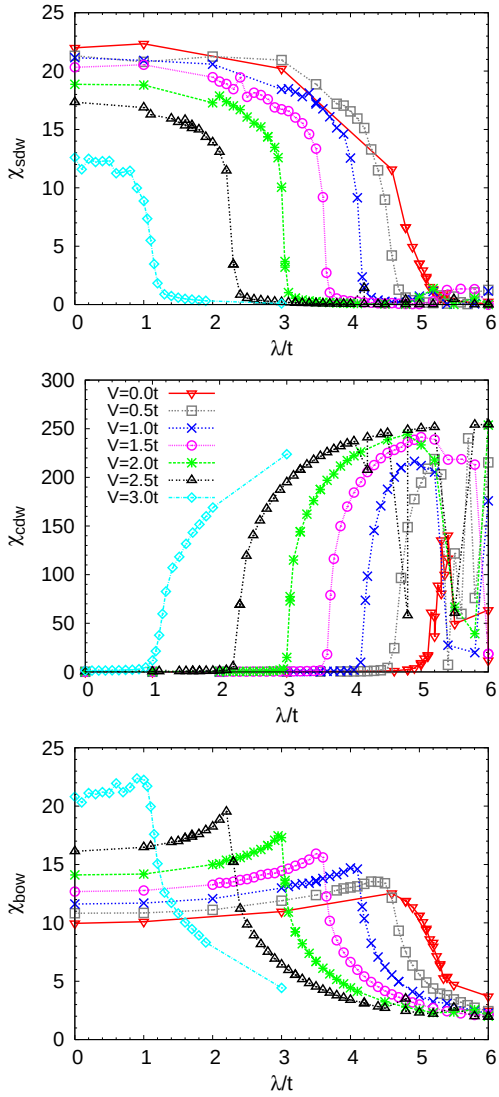

FIG. 7: Spin-density wave (top), charge-density wave (middle), and bond-ordered wave (bottom) susceptibilities versus electron-phonon coupling λ for $U = 6t$, $V = 0.0t, (0.5t), 3.0t$, $\omega_0 = 2t$, and $N = 32$.

tonians and are associated with long equilibration times which occur when the electrons and lattice degrees of freedom are strongly coupled.

As with $\widehat{H}_{\rm ihm}$, the components of the energy (Fig. 8) lend important supporting evidence for the locations of the transition points. The behavior of E_V and E_U is the same as that observed previously in Fig. 3, and is more or less clear: in the SDW phase most sites are singly occupied and there is a significant contribution to E_V, which then drops abruptly in the CDW phase where doubly occupied and empty sites alternate. In contrast, E_U is small in the SDW phase since sites are singly occupied, but then increases sharply in the CDW phase. What is perhaps less intuitive is the evolution of the phonon contributions to the energy. As λ grows, the $t = 0$ analysis suggests a smooth quadratic increase, $\mathrm{PE}_{\rm phonon} = \lambda^2/2\omega_0^2$. Instead the phonon potential energy remains relatively flat throughout the SDW region, and then jumps up as the CDW is entered. The phonon kinetic energy is especially interesting, showing a well-defined *minimum* in the transition region. The origin of this effect is not clear. $\mathrm{KE}_{\rm phonon}$ is measured by the fluctuations of the phonon coordinates in imaginary time. Naively, one might expect kinetic lattice fluctuations to be *largest* in the SDW-CDW transition region where the system is undecided between which type of order to assume. In the case of the electron kinetic energy we see precisely this effect in Fig. 8(a). The opposite appears to be the case for the phonon kinetic energy.

Finally, Fig. 9 shows the phase diagram in the $V - \lambda$ plane at fixed $U = 6t$. It shares the same general features as Fig. 5 with a SDW phase near the origin

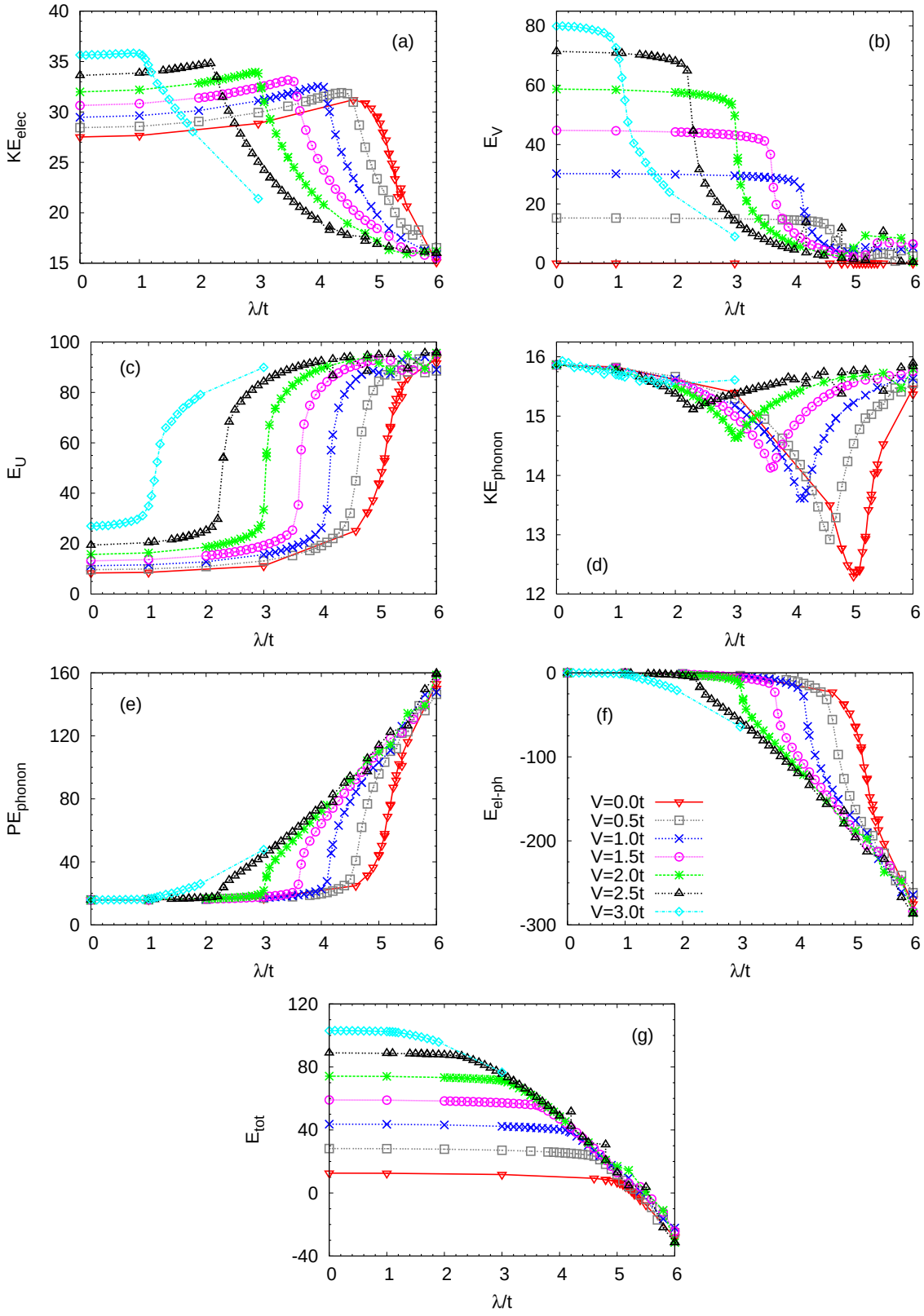

FIG. 8: (a) Kinetic (hopping), (b) intersite Coulomb, (c) on-site Coulomb, (d) kinetic (phonon), (e) potential (phonon), (f) electron-phonon coupling, and (g) total energies versus coupling constant λ for $U = 6t$, $V = 0.0t(0.5t), 3.0t$, $\beta t = 8$, $\omega_0 = 2t$, and $N = 32$. The fluctuations in the phonon kinetic energy are significantly smaller than those for all other energies for these parameters.

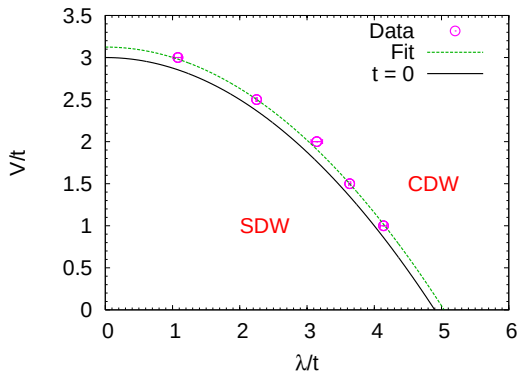

FIG. 9: This figure shows the phase diagram for intersite V and electron-phonon coupling λ with $U = 6t$, $\omega_0 = 2t$, and $\beta t = 8$. Line with symbols is the result of the WLQMC simulations in this paper. The functional form of the fit is $V = a\lambda^2 + b$. We show the exact result (line without symbols) for the $t = 0$ phase.

that is destroyed when either the intersite repulsion V or the electron phonon coupling λ increases sufficiently. It is important to note that, unlike Fig. 5, the QMC phase boundary does not bend away from the $t = 0$ line $V_c = U/2 - \lambda^2/4\omega_0$. Instead, the boundary is uniformly shifted to increase the critical intersite repulsion, favoring SDW order. Again, the $\lambda = 0$ point on our phase boundary ($V_c = 3.124 \pm 0.011$) agrees well with Jeckelmann's DMRG treatment. (See above discussion of Fig. 5.)

For finite λ we can compare against the phase diagram of Sil and Bhattacharyya who study the same extended Hubbard model coupled to Holstein phonons[38]. They draw the phase boundary in the $U - V$ plane for different electron phonon couplings. Translating to the units used in our paper, for $U = 6t$ and $V = 2t$, their data suggests that the CDW phase is destroyed at $\lambda_c \approx 2.8$. Our Fig. 9 gives $\lambda_c \approx 3.0$ at $V = 2t$ for the same parameters. Likewise, Sil and Bhattacharyya find that for $\lambda = 5.6$ there is no SDW phase at $U = 3t$. This is again nicely consistent with our data which suggest that when $\lambda = 5.04 \pm 0.06$ there is CDW order.

V. SUMMARY

In this paper we have presented World Line Quantum Monte Carlo simulations of the extended one-dimensional Hubbard Hamiltonian to which coupling to static staggered (ionic Hubbard) or dynamic (Holstein) lattice degrees of freedom is added. The evolution of the susceptibilities to different types of order and the components of the energy were examined. For both static and dynamic couplings the region of charge density wave order in the phase diagram is found to be stabilized, and the phase boundaries are pinned down. Bond order is shown to be enhanced in the vicinity of the spin density to charge density transition.

The results obtained in this work also show good agreement with previous studies. The zero-coupling limit ($\Delta, \lambda = 0$) results conform well with Jeckelmann's DMRG results. For dynamic couplings, the results compare favorably with the results of Sil *et al.*

A comparison of the QMC phase boundaries with their counterpart in the $t = 0$ limit shows a markedly different behavior between the two types of couplings. For static couplings, the CDW phase is enhanced in the QMC calculation. Conversely, there is an enhancement of the SDW correlations with Holstein phonons.

We acknowledge support from the National Science Foundation under awards DOE DE-FG01-06NA26204 and NSF REU PHY-0243904, and useful input from G.K. Pips.

[1] H. G. Keiss, ed., *Conjugated Conducting Polymers* (Springer-Verlag, Berlin, 1992).
[2] T. Ishiguro and K. Yamaji, *Organic Superconductors* (Springer-Verlag, Berlin, 1990).
[3] V. J. Emery, in *Highly Conducting One Dimensional Solids*, edited by J. Devreese, R. Evrard, and V. van Doren (Plenum, New York, 1979).
[4] J. Sólyom, Adv. Phys. **28**, 201 (1979).
[5] J. E. Hirsch, Phys. Rev. Lett. **53**, 2327 (1984).
[6] J. E. Hirsch, Phys. Rev. B **31**, 6022 (1985).
[7] J. W. Cannon and E. Fradkin, Phys. Rev. B **41**, 9435 (1990).
[8] J. W. Cannon, R. T. Scalettar, and E. Fradkin, Phys. Rev. B **44**, 5995 (1991).
[9] M. Nakamura, J. Phys. Soc. Japan **68**, 3123 (1999).
[10] M. Nakamura, Phys. Rev. B **61**, 16377 (2000).
[11] P. Sengupta, A. W. Sandvik, and D. K. Campbell, Phys. Rev. B **65**, 155113 (2002).
[12] The model with random, rather than alternating, static distortions is often referred to as the 'binary alloy Hubbard Hamiltonian'. The possibility of a Mott transition away from half-filling has recently been discussed, see Reference 15.
[13] S. S. Kancharla and E. Dagotto, Phys. Rev. Lett. **98**, 016402 (2007).
[14] N. Paris, K. Bouadim, F. Hebert, G. G. Batrouni, and R. T. Scalettar, Phys. Rev. Lett. **98**, 046403 (2007).
[15] K. Byczuk, M. Ulmke, and D. Vollhardt, Phys. Rev. Lett. **90**, 196403 (2003).
[16] K. Byczuk, W. Hofstetter, and D. Vollhardt, Phys. Rev. B **69**, 045112 (2004).
[17] A. Garg, H. R. Krishnamurthy, and M. Randeria, Phys. Rev. Lett. **97**, 046403 (2006).
[18] D. Jaksch, C. Bruder, J. I. Cirac, C. W. Gardiner, and P. Zoller, Phys. Rev. Lett. **81**, 3108 (1998).
[19] P. Buonsante and A. Vezzani, Phys. Rev. A **70**, 033608 (2004).
[20] P. Buonsante, V. Penna, and A. Vezzani, Phys. Rev. A **70**,

061603 (2004).
[21] P. Buonsante and A. Vezzani, Phys. Rev. A **72**, 013614 (2005).
[22] V. G. Rousseau, D. P. Arovas, M. Rigol, F. Hebert, G. G. Batrouni, and R. T. Scalettar, Phys. Rev. B **73**, 174516 (2006).
[23] N. R. Thomas, A. C. Wilson, and C. J. Foot, Phys. Rev. A **65**, 063406 (2002).
[24] S. Friebel, C. D'Andrea, J. Walz, M. Weitz, and T. W. Hänsch, Phys. Rev. A **57**, R20 (1998).
[25] P. Ahmadi, V. Ramareddy, and G. S. Summy, New J. Phys. **7**, 4 (2005).
[26] S. Peil, J. V. Porto, B. L. Tolra, J. M. Obrecht, B. E. King, M. Subbotin, S. L. Rolston, and W. D. Phillips, Phys. Rev. A **67**, 051603 (2003).
[27] J. Hubbard and J. B. Torrance, Phys. Rev. Lett. **47**, 1750 (1981).
[28] T. Egami, S. Ishihara, and M. Tachiki, Science **261**, 1307 (1993).
[29] G. Ortiz and R. M. Martin, Phys. Rev. B **49**, 14202 (1994).
[30] R. Resta and S. Sorella, Phys. Rev. Lett. **74**, 4738 (1995).
[31] R. Resta and S. Sorella, Phys. Rev. Lett. **82**, 370 (1999).
[32] M. Fabrizio, A. O. Gogolin, and A. A. Nersesyan, Phys. Rev. Lett. **83**, 2014 (1999).
[33] T. Wilkens and R. M. Martin, Phys. Rev. B **63**, 235108 (2001).
[34] C. D. Batista and A. A. Aligia, Phys. Rev. Lett. **92**, 246405 (2004).
[35] Y. Z. Zhang, C. Q. Wu, and H. Q. Lin, Phys. Rev. B **66**, 035115 (2002).
[36] Y. Z. Zhang, C. Q. Wu, and H. Q. Lin, Phys. Rev. B **67**, 205109 (2003).
[37] J. Riera and D. Poilblanc, Phys. Rev. B **62**, R16243 (2000).
[38] S. Sil and B. Bhattacharyya, Phys. Rev. B **54**, 14349 (1996).
[39] J. E. Hirsch, R. L. Sugar, D. J. Scalapino, and R. Blankenbecler, Phys. Rev. B **26**, 5033 (1982).
[40] H. F. Trotter, Proc. Am. Math. Soc. **10**, 545 (1959).
[41] M. Suzuki, Phys. Lett. A **113**, 299 (1985).
[42] R. M. Fye, Phys. Rev. B **33**, 6271 (1986).
[43] R. M. Fye and R. T. Scalettar, Phys. Rev. B **36**, 3833 (1987).
[44] M. Barma and B. S. Shastry, Phys. Rev. B **18**, 3351 (1978).
[45] A. W. Sandvik and J. Kurkijärvi, Phys. Rev. B **43**, 5950 (1991).
[46] A. W. Sandvik, J. Phys. A **25**, 3667 (1992).
[47] A. W. Sandvik, Phys. Rev. B **59**, R14157 (1999).
[48] N. V. Prokof'ev, B. V. Svistunov, and I. S. Tupitsyn, J. Expt. and Theor. Phys. **87**, 310 (1998).
[49] In addition to moves which change a phonon coordinate at a single space-time point we also include moves which modify the phonon coordinates at all imaginary times for a given spatial site.
[50] A. W. Sandvik, P. Sengupta, and D. K. Campbell, Phys. Rev. Lett. **91**, 089701 (2003).
[51] E. Jeckelmann, Phys. Rev. Lett. **89**, 236401 (2002).
[52] E. Jeckelmann, Phys. Rev. Lett. **91**, 089702 (2003).